Published in final edited form as:
Mol Pharm. 2013 December 2; 10(12): 4560–4571. doi:10.1021/mp400371r.

Biodistribution of Fluorescently Labeled PAMAM Dendrimers in Neonatal Rabbits: Effect of Neuroinflammation

Wojciech G. Lesniak[†], **Manoj K. Mishra**[†], **Amar Jyoti**[‡], **Bindu Balakrishnan**[‡], **Fan Zhang**[†], **Elizabeth Nance**[‡], **Roberto Romero**[§], **Sujatha Kannan**[‡], and **Rangaramanujam M. Kannan**[*,†]

[†]The Center for Nanomedicine, Department of Ophthalmology, Johns Hopkins School of Medicine, Baltimore, Maryland 21287, United States

[‡]Department of Anesthesiology and Critical Care Medicine, Johns Hopkins University School of Medicine, Baltimore, Maryland, 21287, United States

[§]Perinatology Research Branch, NICHD, NIH, DHHS, Detroit, Michigan, 48201, United States

Abstract

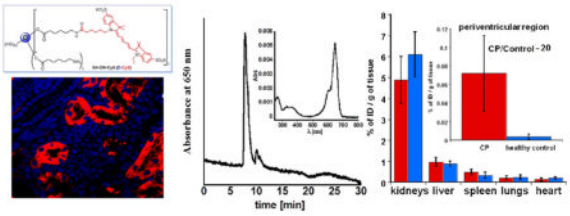

Dendrimers are being explored in many preclinical studies as drug, gene, and imaging agent delivery systems. Understanding their detailed organ, tissue, cellular uptake, and retention can provide valuable insights into their effectiveness as delivery vehicles and the associated toxicity. This work explores a fluorescence-quantification based assay that enables simultaneous quantitative biodistribution and imaging of dendrimers with a single agent. We have labeled an ethylenediamine-core generation-4 hydroxyl-terminated poly(amidoamine) (PAMAM) dendrimer using the fluorescent photostable, near-IR cyanine dye (Cy5) and performed quantitative and qualitative biodistribution of the dendrimer-Cy5 conjugates (D-Cy5) in healthy neonatal rabbits and neonatal rabbits with cerebral palsy (CP). The biodistribution of D-Cy5 and free Cy5 dye was evaluated in newborn rabbits, based on the developed quantification methods using fluorescence spectroscopy, high-performance liquid chromatography (HPLC), and size exclusion chromatography (SEC) and supported by microscopic imaging. The uptake was assessed in the brain, heart, liver, lungs, kidneys, blood serum, and urine. Results obtained based on these three independent methods are in good agreement and indicate the fast renal clearance of D-Cy5 and free Cy5 with relatively higher organs accumulation of the D-Cy5 conjugate. Following systemic administration, the D-Cy5 mainly accumulated in kidneys and bladder at 24 h. The quantitative biodistribution is in good agreement with previous studies based on radiolabeling. These methods for dendrimers quantification are easier and more practical, provide excellent sensitivity (reaching

[*]Corresponding Author: Tel.: +443-287-8634. krangar1@jhmi.edu.

Notes

The authors declare no competing financial interest.

Supporting Information

Fluorescence excitation and emission, HPLC characterization, size exclusion chromatographs, and urine samples. This material is available free of charge via the Internet at http://pubs.acs.org.

0.1 ng per gram of tissue), and allow for quantification of dendrimers in different organs over longer time periods without concerns for radioactive decay, while also enabling tissue and cellular imaging in the same animal. In kits with fetal-neuroinflammation induced CP, there was a significantly higher uptake of D-Cy5 in the brain, while biodistribution in other organs was similar to that of healthy kits.

Keywords

PAMAM dendrimer; biodistribution; brain uptake quantification; cellular imaging; pharmacokinetics; neuroinflammation; cerebral palsy

INTRODUCTION

Poly(amidoamine) (PAMAM) dendrimers are emerging as promising candidates for the development of multifunctional targeted delivery nanodevices for diagnosis and treatment of cancer,[1–10] rheumatoid arthritis,[11,12] and inflammation.[13–20] Their globular nature (3–12 nm), branching architecture, and high density of tailorable surface groups that can be modified to achieve desired physicochemical properties, provide significant advantages for these applications. PAMAMs can be prepared to be nontoxic, with multiple peripheral functional groups, for the conjugation of drugs, targeting, imaging, radioactive, and chelating agents.[2,3,13,21–23] It has been shown that the circulation time, organ biodistribution, and passive tumor targeting depend strongly on the physicochemical properties of the dendrimers, extent of PEGylation, presence of ligands, and dendrimer–protein interactions.[24–30]

We have previously explored dendrimer-based drug delivery in cerebral palsy (CP), which is a debilitating childhood disorder with no effective cure. Neuroinflammation is a leading cause of CP, as well as many other debilitating neurological disorders.[13] Recent studies have also shown that intravenous administration of hydroxyl-terminated generation-4 PAMAM dendrimer, without targeting ligands, results in increased uptake in the brain of newborn rabbits with neuroinflammation and leads to their selective localization in activated microglia and astrocytes in the brain of neonatal rabbits with CP, but not in age-matched healthy controls.[13] We have previously reported that hydroxyl-functionalized generation-4 PAMAM dendrimer (G4-OH) does not induce any liver and kidney toxicity even at a dose of 550 mg/kg in the healthy neonatal rabbit.[13] Hence, these nanoparticles may be safely used as vehicles for targeted drug delivery. Importantly, a single dose of dendrimer-*N*-acetyl cysteine conjugate (D-NAC) (10 mg/kg) administered intravenously on the day of birth to rabbit kits with CP resulted in a significant improvement in motor function, decrease in oxidative stress, attenuation of activated microglia, and decrease in neuronal injury by 5 days of age.[13–15] Previous studies with PAMAM dendrimers showed that they accumulated in sentinel nodes allowing for their imaging by both MRI and optical modalities, suggesting potential applicability as mapping and guidance agents before and during surgery, respectively.[10]

Considering the large body of research on the biomedical applications of PAMAM dendrimers, development of convenient methods for their biodistribution and pharmacokinetic studies, along with tissue imaging, would be of great interest. To date, a majority of the biodistribution and pharmacokinetic studies of PAMAM dendrimers have been performed using radioactive labeling with isotopes such as ^{3}H, ^{111}indium, ^{88}yttrium, ^{153}gadolinium, and ^{125}iodine.[21,24–30] These studies have collectively demonstrated the importance of size and surface properties on the biodistribution of PAMAM dendrimers. PAMAM dendrimer below generation six are

rapidly cleared from the systemic circulation by kidney filtration (neutral) or reticuloendothelial system (positively charged). PEGylated dendrimers or higher generation dendrimers (six and above) tend to circulate longer and evenly distribute within major peripheral organs. In addition, only trace amounts were reported to be transported across an intact blood–brain barrier.[24–30]

Although radioactive labeling provides high sensitivity and reliable results, near-IR fluorescence quantification can provide additional benefits, such as low limit of detection reaching femtomoles, photostability, relatively easy sample handling, analysis using common modalities including fluorescence spectrophotometers, plate readers, or optical scanners. In addition, the same probe could also enable near-IR tissue/cell imaging of dendrimers. This study explores the use of near-IR labeling agent (Cy5) conjugated to the dendrimer (D-Cy5) to: (a) quantify and image dendrimer biodistribution and (b) study how the biodistribution is affected by the presence of neuroinflammation.

MATERIALS AND METHODS

Materials and Reagents

Ethylenediamine-core poly-(amidoamine) [PAMAM] hydroxyl-terminated generation-4 dendrimer [G4(OH)$_{64}$] was purchased from Dendritech Inc., MI. Benzotriazol-1-yl-oxytripyrrolidinophosphonium hexafluorophosphate (PyBOP), methanol (MeOH), formalin, acetonitrile (ACN), trifluoroacetic acid (TFA), 6-(Fmoc-amino)caproic acid, and chloroform were purchased from Sigma-Aldrich (St. Louis, Missouri). Cy5-mono-NHS ester was purchased from Amersham Biosciences-GE Healthcare. Triethylamine (TEA) and diisopropylethylamine (DIEA) were purchased from Thermo Fisher Scientific Inc. (Pittsburgh, Pennsylvania). Dimethylformamide (DMF) and dimethyl sulfoxide (DMSO) were purchased from EMD Chemicals (Gibbstown, New Jersey). TSK gel ODS-80 Ts (250 4.6 mm, i.d., 5 μm) and TSK gel guard column were bought from Tosoh Bioscience LLC. Size exclusion Ultrahydrogel 120 (7.8 mm × 300 mm) column and Ultrahydrogel DP (6 mm × 40 mm) guard column were purchased from Waters Corporations. Water used in all experiments was purified by a Branstead Nanopure Diamond Lab water purification system with a resistivity of 18.2 MΩ cm^{-1}. All reagents and solvents were HPLC grade and were used as received without further purification. For confocal microscopy, nuclei counterstain, DAPI (4′,6-diamidino-2-phenylindole, dihydrochloride) and Vectashield mounting media were purchased from Invitrogen. Regenerated cellulose (RC) dialysis membrane with molecular weight cutoff of 1000 Da was obtained from Spectrum Laboratories Inc. (Rancho Dominguez, California).

Proton NMR Characterization—Proton NMR spectra of the intermediates and D-Cy5 were recorded on a Bruker (500 MHz) spectrometer using commercially available DMSO-d_6 solvents. Proton chemical shifts were reported in ppm (δ) and tetramethylsilane (TMS) used as an internal standard.

Fluorescence Spectroscopy (FLS)—Fluorescence spectra of free Cy5 and D-Cy5 were recorded in methanol and phosphate buffer (0.1M), using a Shimadzu RF-5301 spectrofluorometer. To obtain calibration curves and to determine the limits of detection for Cy5 and D-Cy5, their emission spectra (with excitation at 645 nm) were recorded at concentrations ranging from 1 ng/mL to 100 μg/mL and appropriate sets of excitation and emission slit widths. Depending on either Cy5 or D-Cy5 level in biological samples different calibration curves with appropriate slit widths were used for their quantification. For quantification of D-Cy5 in kidney and urine, the excitation and emission slit widths were set to 3 and 5, whereas for other tissue specimens, both slits were set to 10. To

compensate for autofluorescence originating from the tissue at the near-IR wavelength, intensity registered for control tissue samples from untreated rabbits was subtracted from the values observed for tissue samples acquired from rabbits injected with either D-Cy5 or Cy5.

High-Performance Liquid Chromatography (HPLC)—Cy5, D-Cy5 conjugate, and the extracts from tissue specimen were analyzed using a Waters 1525 binary HPLC separation module, equipped with a Waters In-Line degasser AF, a Waters 717 plus autosampler (kept at 4 °C), a Waters 2998 photodiode array detector, a Water 2475 multi λ fluorescence detector, controlled by a Waters Empower software. Gradient separations were run on TSK-Gel ODS-80 Ts (250 4.6 mm, i.d., 5 μm) and TSK-Gel guard columns with 0.1% (v/v) TFA inH_2O–ACN starting ratio 90:10 (v/v) increasing linearly to 10:90 in 30 min at a flow rate of 1 mL/min. Triplicated injections for each analyzed sample were performed. Elution was simultaneously monitored by PDA detector (collecting UV–vis spectra from 190 to 800 nm every 2 s that allows for obtaining chromatograms at the desired wavelength in this range) as well as a fluorescence detector, having one channel set for detection of Cy5 with excitation at 645 nm and emission at 662 nm. To obtain calibration curves and determine the limits of detection (LOD) for Cy5 and D-Cy5, different amounts of the dye and conjugate (ranging from 1 ng to 100 μg) were injected on the column and used as external standards for their quantification in rabbit organs, blood serum, and urine.

Size Exclusion Chromatography (SEC)—Analysis of the starting dendrimer, all intermediates, the final D-Cy5 conjugate, and extracts was performed using the same HPLC system as described above with both PDA and fluorescent detectors. However, Waters size exclusion Ultrahydrogel 120 7.8 × 300mm and Ultrahydrogel DP 6 × 40 guard columns, and an isocratic elution with phosphate buffer (0.1 M, pH 7.4) and 0.025% sodium azide were used. The flow rate was maintained at 0.6 mL/min. Different amounts of D-Cy5 ranging from 1 ng to 100 μg were injected on the column to construct calibration curves and estimate LOD.

Method Development for Quantification of D-Cy5—We exploited a combination of FLS, HPLC, and SEC methods to quantify the D-Cy5 conjugate and free Cy5 in biological specimens. To test limit of detection (LOD), solutions containing D-Cy5 at concentration ranging from 100 pg/mL to 1 μg/mL were analyzed by FLS, HPLC, and SEC as described above. The highest sensitivity for detection of D-Cy5 reaching a concentration of 100 pg/mL was observed for FLS. LODs for D-Cy5 analyzed by HPLC and SEC were 0.1 μg and 0.01 μg injected on the column, respectively. The observed difference in LOD for HPLC and SEC may be due to the use of different mobile phases. SEC was run with phosphate buffer at a concentration of 0.1 M and pH = 7.4 as the mobile phase, and for HPLC analysis, gradient elutions with 0.1% (v/v) of TFA in H_2O and ACN (pH ~ 2.5) were carried out. Protonation of Cy5 resulted in a significant increase of LOD. Many different extraction procedures of D-Cy5 conjugate from all analyzed tissue samples were evaluated including homogenization in PBS, methanol, and H_2O–MeOH solutions at 50:50 and 25:75 ratios, as well as different kinds of tubes such as regular Eppendorf vials, glass vials, siliconized glass tubes, and low DNA binding tubes. The best recovery reaching around 95% of all tested organs (brain, liver, kidney, heart, and lung) was observed for extraction with MeOH in the low DNA binding tubes. Recovery rates were tested using external calibration curves obtained for D-Cy5 at different concentration ranges depending on a known amount of injected D-Cy5 into the tissue samples, which was estimated based on previously published biodistribution studies with radioactive labeling.,[24–31] At all concentration ranges, calibration curves exhibited excellent linearity with $R = 0.998$. To test the reproducibility of the developed methods, standard solutions in PBS buffer containing D-Cy5 or Cy5 at concentration of 10 μg/mL was aliquoted into 10 samples, which were stored at −20 °C.

Intra- and interday variations were evaluated by measuring these aliquots on 10 consecutive days, using freshly thawed samples every day. Each sample was analyzed in triplicate. No statistically significant differences for daily and day-to-day analysis in terms of signal intensity in fluorescence spectroscopy and peak areas in the case of HPLC and SEC were observed. The same approach was applied to extract Cy5 and determine its concentration by FLS and HPLC.

Animals—All animal procedures were approved by the Institutional Animal Care and Use Committee. Female New Zealand white rabbits were obtained from Robinsons Service Inc. Mocksville, NC, USA and bred in-house at the animal facility of the Johns Hopkins School of Medicine. Pregnant rabbits were allowed to deliver kits at term on gestation day 31.

Rabbit Kits with Cerebral Palsy—Pregnant rabbits underwent laparotomy at gestational day 28 (term pregnancy 31 days) under general anesthesia (2–3% isoflurane by mask) and were injected with 1 mL of saline containing 20 μg/kg of *E. coli* endotoxin (*Escherichia coli* serotype O127:B8, Sigma Aldrich) along the length of the uterus as previously described by us.[13] Kits born to dams exposed to endotoxin *in utero* displayed motor deficits suggestive of cerebral palsy as previously described, characterized by robust neuroinflammation, and mediated by activated microglia.[13]

Newborn kits were fed rabbit formula (Wombaroo, milk replacement products for mammals, Belleville, MI) three times a day at 150 mL/kg/day. On postnatal day5, kits were injected with D-Cy5 (N = 5) or free Cy5 (N = 5) intravenously at a dose of 800 μg per animal on a Cy5 basis. Kits were sacrificed 24 h later after a lethal dose of pentobarbital, and blood (transcardially) and urine (directly from bladder) were collected. The kits were then *perfused with PBS* to remove blood from different organs. Brain, liver, spleen, kidneys, lungs, and heart were collected from each animal and divided into two portions; one part was snap frozen on dry ice and stored at −80 °C for quantification of Cy5 and D-Cy5, and the other part was kept in formalin to fix the tissue and process for cryosectioning.

Extraction Procedure—Approximately 100–150 mg of frozen tissue was homogenized in 1 mL of methanol with TissueLyser LT, Giagen homogenizer in 2mL DNA LoBind eppendorf tubes. Resulting suspensions were extensively vortexed and sonicated. Appropriate volumes of obtained suspensions containing 100 mg of tissue were placed in different vials and diluted with methanol up to 1 mL, to keep the same amount of tissue and the same volume for each sample. Homogenized samples were then centrifuged at 10 000 rpm for 10 min at 4 °C. Resulting supernatants were subjected to fluorescence spectroscopy. After collecting spectra, methanol was evaporated, and obtained residues were dissolved in DI water, filtered using 0.2 μM filters, and analyzed by HPLC and SEC. The amount of D-Cy5 and Cy5 in tissue was expressed as micrograms of dendrimer per grams of organ weight (μg/g). A sample of 100 μL of urine or blood serum was mixed with 900 μL of phosphate buffer (c = 0.1M), filtered using 0.2 μM filters, and analyzed by fluorescence spectroscopy, HPLC, and SEC. Concentrations of the D-Cy5 conjugate and Cy5 in urine and blood were expressed in microgram of analyte per milliliter (μg/mL).

Tissue Processing for Imaging—Formalin-fixed samples were washed with PBS and then made isotonic with 30% sucrose in PBS by passing through sucrose gradients. Tissues were then snap-frozen, and 30 μm thick sections were obtained using Leica CM 1950 cryostat. Cryosections were kept frozen at −20 °C until staining was initiated. Five slides (3 sections per slide, total of 15 sections per animal) from the same regions of each organ from different animals were briefly washed with PBS and then incubated with DAPI (Sigma-Aldrich) in PBS for 10 min to counter stain nuclei and mounted with Vectashield mounting

media (Vector lab. Burlingame, CA, USA). Blinded sections were imaged with the help of advance confocal LSM 710 microscope (Carl Zeiss; Hertfordshire, UK) for accumulation of the dendrimers in different organs. Cy5 (free and conjugated forms) was imaged by exciting fluorophore 633 lasers with a laser power kept at 2.0 and a pinhole set at 1. Background fluorescence was eliminated by setting up laser thresholds from the tissues of animals which were not injected with either free Cy5 or D-Cy5. Keeping the settings exactly identical, images (1026 × 1026) were acquired for different groups of animals with the help of Zen 2011 software (Carl Zeiss MicroImaging GmbH, Jena, Germany). Images were acquired at 10× and 40× magnifications for qualitative comparisons; however, for clarity only 40× images are shown. To confirm the locations where the fluorescence images were taken, corresponding slides were stained with hematoxylin and eosin (Sigma-Aldrich, St. Louis, MO, USA). Images were captured with the help of a Nikon inverted microscope (Nikon Instrumentation Inc., Melville, NY).

RESULTS

Synthesis and Physicochemical Characterization

To prepare the D-Cy5 conjugate, we partially modified generation four hydroxyl-terminated PAMAM dendrimer (D) with reactive amine surface end groups shown in Scheme 1. The resulting bifunctional dendrimer was reacted with *N*-hydroxysuccinimide monoester Cy5 dye to obtain the D-Cy5 conjugate. The detailed synthetic procedure for the preparation of the bifunctional dendrimer and its physicochemical characterization was described previously.[14] In brief, the Fmoc-protected amine linker, 6-(Fmoc-amino)caproic acid was reacted with the dendrimer in the presence of PyBOP coupling reagent under basic conditions to produce Fmoc-protected dendrimer intermediate. The intermediate was characterized by ^{1}H NMR, and the average loading of the Fmoc-aminocaproic acid to the dendrimer surface was calculated by integration of appropriate signals seen in ^{1}H NMR. Comparison of the signal of amidic proton of the dendrimer and aromatic proton of the Fmoc groups indicated that four linker molecules were conjugated to the dendrimer. The Fmoc groups of the Fmoc-protected intermediate were eliminated using piperidine/DMF mixture (2:8) to get free primary amine groups on the surface of the dendrimer, which facilitates the reaction with NH_2-reactive Cy5-NHS ester dye. The final conjugate was purified by dialysis followed by GPC fractionation. The resulting conjugate was extensively analyzed by proton NMR, HPLC/GPC, DLS, and fluorescence spectroscopy. In the ^{1}H NMR spectrum appearance of methylene protons peaks (1.2–2.1 ppm) and aromatic protons peaks (6.3–8.4) of Cy5 along with dendrimer and linker protons peaks confirm the formation of the conjugate (Figure 1).

Conjugation of Cy5 to the dendrimer did not alter its fluorescence spectrum, and the resulting conjugate could be excited at 645 nm with maximum of emission at 662 nm (Supporting Information, Figure 1S and Figure 2). The D-Cy5 exhibits high fluorescent yield, allowing for its detection at concentrations as low as 100 pg/mL in methanol or phosphate buffer at pH = 7.4, using a Shimadzu RF-5301 spectrofluorometer with both excitation and emission slit width set to 10. The purity and size of D-Cy5 were evaluated by HPLC and SEC, equipped with PDA and fluorescence detectors (Supporting Information: Figure 2S, 3S and Figures 3A and 4A,B). In both chromatographic methods, D-Cy5 was detected by absorbance at 650 nm and fluorescence (ex. 645 nm/em. 662 nm). In case of HPLC, the same elution and detection conditions could be used to analyze D-Cy5 and free Cy5 since their elution times were different. Peaks related to the conjugate and free dye exhibited satisfactory baseline separation and could be analyzed concurrently, as confirmed by the analysis of the physical mixture of D-Cy5 and Cy5 (Supporting Information, Figure 2S) and separately (Figure 3A and D). It is worth noting that HPLC of the free Cy5 shows

the presence of two fluorescence species indicating around 75% purity, which in good agreement with manufacturer specifications. Results obtained for D-Cy5 based on size exclusion chromatography confirmed that the conjugate exhibits narrow size distribution. HPLC and SEC indicated a high purity of D-Cy5. The UV–visible spectrum of the conjugate (Figures 3 and 4 inserts) was useful in peak assignment during quantification of the conjugate in biological specimens. In addition, both methods confirmed covalent attachment of Cy5 to the dendrimer since they migrate together through columns and peak related to D-Cy5 revealed UV–visible pattern characteristic for Cy5.

Stability of D-Cy5 Conjugate

The stability of D-Cy5 conjugate in PBS and human plasma was evaluated. D-Cy5 was incubated for 24 h in PBS or/and human plasma at 37 °C, and the signal intensity as well as peak areas in HPLC and SEC chromatograms did not change. We also tested the possibility of dendrimer interactions with constituents of human plasma. In this case the D-Cy5 was mixed with plasma and analyzed without any additional steps by SEC equipped with two in-line Ultrahydrogel columns and phosphate buffer (c = 0.1 M and pH = 7.4) as a mobile phase. As presented in Figure 5, the intensity and retention time of signals related to plasma constituents and D-Cy5 did not change upon mixing. The same SEC profile for the system composed of human plasma and D-Cy5 was observed after 24 h of their incubation at 37 °C, suggesting that the conjugate was stable under these conditions. Also, there were no additional peaks that would indicate the formation of other species with dendrimer, especially bigger agglomerates that would appear at shorter retention time. These results suggest that D-Cy5 is stable for at least 24 h in plasma at 37 °C and that the hydroxyl-functionalized dendrimer did not form stable aggregates with plasma proteins at pH 7.4 which could be detected with this method.

Biodistribution and Excretion of D-Cy5 and Cy5

Free Cy5 or D-Cy5 conjugate were injected intravenously through a peripheral vein in neonatal healthy rabbit kits on postnatal day 5 for quantitative and qualitative biodistribution studies. The major organs such as kidney, lungs, liver, heart, and brain, as well as blood serum and urine (obtained from bladder), were analyzed 24 h after systemic administration for the presence of Cy5 in free and D-Cy5 conjugate forms. For accuracy, the concentrations of D-Cy5 in specimens were measured using three independent methods including FLS (Figure 2), HPLC (Figure 3), and SEC (Figure 4). The concentration of free dye was evaluated based on fluorescence spectroscopy and HPLC (Figures 2 and 3). As can be seen in Figure 2, FLS confirmed that applied extraction protocol of D-Cy5 and Cy5 from kidneys, using methanol, yielded a solution exhibiting their respective fluorescence properties. Both spectra recorded at the same excitation and emission slit widths indicate significantly higher intensity in D-Cy5 administered rabbits. A similar pattern was observed for other analyzed specimens. A negligible background signal in Cy5 channel could be observed for extracts obtained using organs from control (nontreated) animals. The identity of the species observed by FLS was further tested and validated by HPLC and SEC (Figures 3 and 4). D-Cy5 and Cy5 could be detected using both PDA and fluorescence detectors. The HPLC and SEC chromatograms (including peak shape, its retention, and UV–visible spectral pattern under peak) of D-Cy5 used as a standard, and that extracted from kidney or present in the urine samples was identical, indicating that the conjugate was stable *in vivo* and the applied extraction procedure left the conjugate intact. In addition, the HPLC analysis of urine samples obtained from rabbits injected with D-Cy5 (example shown in Figure 3C) indicated that only a small amount of free Cy5 was released from the conjugate (3% of the total amount of Cy5 injected in the form conjugated to dendrimer, based on calibration curves for free Cy5 and D-Cy5). The release may be due to hydrolytic or enzymatic cleavage of ester bonds between the linker and hydroxyl groups of dendrimer. A trace

amount of free Cy5 (1.82×10^{-7} g/g, as demonstrated in Figure 3B) in the case of animals treated with D-Cy5 was detected only in the kidneys. Table 1 and Figure 6 summarize the biodistribution data. Results obtained based on all three methods are in good agreement and indicate the fast renal clearance and high bladder accumulation of both Cy5 and D-Cy5 (Figure 6, and Figure 4S in Supporting Information), with a relatively higher organ accumulation of the D-Cy5 compared to free dye 24 h post intravenous (i.v.) injection. The biodistribution and clearance pattern is in good agreement with prior results on PAMAMs biodistribution described based on radiolabeling.[24–30]

After quantitative evaluation of free Cy5 and D-Cy5 in different organs, we assessed the distribution of D-Cy5 in the tissue with confocal microscopy. Organ distribution of the labeled dendrimers (Figure 7) corroborated with what was seen by HPLC, SEC, and FLS. The most D-Cy5 and free Cy5 accumulation was seen in the kidneys at 24 h after administration. D-Cy5 was primarily detected along the epithelial cells of the proximal and distal convoluted tubules of nephrons with very little seen in the glomeruli (Figure 7A). This indicates that the dendrimer is initially rapidly filtered through the glomeruli and may eventually be slowly excreted in the urine from the proximal and distal convoluted tubules. Under similar conditions, free Cy5 accumulation within kidney is considerably less (Figure 7F). In contrast to kidneys, other major organs including liver, lungs, and heart exhibit significantly lower accumulation of D-Cy5; however free Cy5 was undetectable (Figure 7), which is in good agreement with their quantification, described in the previous section. H&E staining shows the cellular organization of different tissue where dendrimer localizations were observed (Figure 7K–O). D-Cy5 or free Cy5 were not detected in the brain parenchyma of these healthy newborn rabbits. Hence it appears that an intact blood–brain barrier (BBB) hinders the dendrimer entry into the brain parenchyma (Figure 7E and J), which is in good agreement with our previous studies[14] and other reports on biodistribution of PAMAM dendrimers, indicating their negligible brain uptake in healthy or tumor bearing animals with an intact BBB.[31]

Biodistribution of the D-Cy5 Conjugate in Healthy and Cerebral Palsy Neonatal Rabbits

We evaluated the biodistribution of D-Cy5 in healthy and CP newborn rabbits administrated with the conjugate on day 1 of life (Table 2 and Figure 8). Our results suggest that there is no significant difference in accumulation of D-Cy5 in major peripheral organs in healthy control and CP animals. Biodistribution of D-Cy5 follows the same pattern as in case of healthy rabbits injected with the conjugate on day 5 of life with the highest accumulation in the bladder and kidneys, confirming its fast renal clearance, even at an earlier age. In contrast, a significant difference in *brain* uptake of D-Cy5 was observed in CP animals, where more than 20-fold (on an average) higher D-Cy5 was detected in the periventricular region of CP kits compared to healthy age-matched control kits. Perfusion with PBS was performed to remove the blood, since the biodistribution of dendrimer was focused on brain tissue uptake, not their presence in the blood. Perfusion was especially critical when quantifying brain uptake, since the extent of uptake is small, and the presence in blood can affect the quantification.[38] It should be noted that the brain accumulation of D-Cy5 is dependent on the extent of the brain injury and the associated neuroinflammation and BBB impairment. We have previously shown that neuroinflammation correlates with the motor deficits and hypertonia in newborn rabbits with CP.[32] The extent of neuroinflammation resulting in brain injury and the severity of CP phenotype is variable between animals and would explain the differences in the dendrimer uptake and the high standard deviation observed. Rabbit kits with a severe CP phenotype (indicated by hypertonia and tone scores of 3–4, and severe motor deficits of the fore limbs and hind limbs) had dendrimer accumulation in the PVR that reached levels of 0.12% of injected dose per gram of tissue (ID/g), 24 h after injection. This is 40-fold higher than those for healthy kits (0.003% ID/g).

However, kits with a milder phenotype that did not have high hypertonia but exhibited motor deficits (tone scores of 1–2) had relatively lower brain uptake (shown in Table 2 and Figure 8).

DISCUSSION

The synthesis protocol yielded a D-Cy5 conjugate, covalently linked to approximately one molecule of Cy5. All analytical results are in good agreement and confirmed that each synthetic step was successful. Proton NMR shows the presence of signals related to all constituents of D-Cy5; the dendrimer, linker, and Cy5 and proton integration of appropriate peaks indicates a molar ratio of 1:4:1, respectively (Figure 1). A number of conjugated functional groups were further confirmed by the change of the molecular weight upon each modification detected using matrix-assisted laser desorption–ionization time-of-flight mass spectrometry (MALDI-TOF). ^{1}H NMR suggests a Cy5 payload of ~4 wt %, indicating that the conjugate molecular mass is still dominated by the PAMAM dendrimer. The size and the zeta potential of the conjugate were similar to that of the free dendrimer, suggesting that the Cy5 did not alter these parameters.

Conjugation of one molecule of Cy5 to the dendrimer was sufficient to obtain relatively low limits of detection for D-Cy5 of 0.1 ng, 10 ng, and 100 ng by fluorescence spectroscopy, SEC, and HPLC, respectively. HPLC and SEC analysis demonstrated the high purity of D-Cy5 nanodevice that can be extracted from the tissue of different organs and detected in the bladder content almost intact, 24 h post intravenous administration (Figure 3, 4). This indicates that the resulting conjugate was stable *in vivo* and could be excreted in the form as injected. SEC analysis (Figure 5) suggested that hydroxyl-terminated D-Cy5 conjugate does not form aggregates with components of human plasma, in contrast to generations 4 and 5 *amine terminated* PAMAMs, which were shown to interact with albumin and erythrocyte acetyl cholinesterase, promoting change in their conformation.[33–35] Interaction of these positively charged dendrimer plasma proteins leads to their opsonization and nonspecific liver and spleen uptake. In contrast, the hydroxyl-terminated D-Cy5 showed predominant accumulation in the kidney, followed by liver, lungs, and heart and was almost undetectable in the *healthy* brain (Table 1 and Figures 6 and 7). In animals administered D-Cy5 and free Cy5, a relatively high concentration of D-Cy5, 263.7 ± 13.0 μg/mL (32.9% of ID), and free dye, 10.62 ± 3.8 μg/mL (35.4% of ID), was detected in the bladder, with much lower concentrations of D-Cy5 (6.48 ± 0.86 μg/mL, 0.81% of ID) and Cy5 (0.43 ± 0.06 μg/mL, 1.43% of ID) in the serum, respectively, at 24 h postinjection. However, much higher organ accumulation was observed for the dendrimer as compared to free dye, most likely due to the longer circulation time and different mechanism of the cellular uptake of globular macromolecules of D-Cy5 and low molecular weight dye. Twenty-four hours after administration of D-Cy5, the relatively low level in blood serum with a high concentration in urine (detectable even with naked eye, since obtained samples were deep green as shown in Supporting Information (Figure 4S), and highest organ accumulation in the kidney suggest rapid renal clearance for both D-Cy5 and Cy5. Excretion results for D-Cy5 are in very good agreement with generation-5 PAMAM dendrimer with acetylamine terminal groups (neutral surface), which undergo faster renal clearance than amine-terminated (positively charged) dendrimer of the same generation.[30] Interestingly, generation-5 hydroxyl-terminated PAMAM dendrimer was shown to exhibit predominant and persistent accumulation in kidneys up to 7 days, most likely due to the larger diameter, compared to generation-4 PAMAMs.[27] The biodistribution pattern and route of excretion of D-Cy5 are in very good agreement with results published in literature, which were obtained based on radioactive labeling of the dendrimer with different isotopes such as ^{3}H and ^{125}I.[24–30] It has been demonstrated that the circulation time, route of elimination, organ accumulation, and passive tumor targeting strongly depends on dendrimers generation (size) and surface

properties including different charge and terminal groups.[24–30] Sadekar et al. showed that hydroxyl-terminated generation-5 PAMAM dendrimers exhibit a short circulation time with predominant accumulation in kidneys, generation 6 is taken up by kidney, liver, and spleen with a slightly longer circulation time, and generation 7 distributes relatively evenly in major organs due to much longer clearance from bloodstream, compared to lower generations.[27] A similar pattern was shown for gadolinium-containing PAMAM dendrimer based MRI contrast agents, where dendrimers with a hydrodynamic size smaller than 6 nm were accumulated in mainly in the kidney and larger than 6 nm were additionally detected in the liver.[36,37] These reports and the fact that renal filtration occurs for particles with hydrodynamic diameter ranging from 3.7 to 6 nm may explain predominant accumulation of D-Cy5 in kidneys, since its size of ~4 nm facilitates renal clearance. The present study suggest that more than 90% of the injected dose of the generation-4 dendrimer is cleared out from the newborn rabbits over 24 h, with less than 5% in blood circulation. Interestingly, even though this dendrimer is shown to distribute into major organs at short times, it appears to be cleared from the organs relatively quickly, which is an ideal feature for preparation of targeted nanoparticles with specific accumulation for imaging or drug delivery.

The increased accumulation of G4 dendrimers in the proximal convoluted tubules, as seen on confocal microscopy in the current study, is in agreement with previous reports.[36] Gd-labeled PAMAM generation-4 OH dendrimer [G4.OH-Gd-(III)], when used as an MRI contrast agent to evaluate renal function, showed increased accumulation in the outer medullary layer (an area where the proximal convoluted tubules are present) in adult mice with normal renal function on MRI. Renal dysfunction resulted in decreased accumulation in this region with decreased urinary clearance of the G4.OH-Gd(III).[36] In our neonatal rabbit model, D-Cy5 was not seen in the glomerulus 24 h after administration, indicating that most D-Cy5 is filtered rapidly from the circulation with slower clearance from the proximal and distal convoluted tubules as seen in the adult mouse model. Confocal images showing relatively higher accumulation of D-Cy5 in kidneys correlates well with the quantification reported from FLS and HPLC, where levels of the conjugate were highest (5% of the injected dose after 24 h) compared to other organs. The quantification data (Table 1 and Figure 6) correspond well with the confocal images of the dendrimer accumulation in organs (Figure 7). We observed that D-Cy5 localizes in the alveolar epithelium of lungs as well as in the liver. Although the magnitude of dendrimer conjugate accumulation is relatively low (less than 1% in 24 h), the dendrimers are readily visualized in the alveoli. The relatively lower liver uptake of D-Cy5 could be a result of minor involvement of the reticulo-endothelial system (RES) in dendrimer clearance, confirmed by the fact that D-Cy5 seems to not interact appreciably with plasma proteins, hence avoiding nonspecific uptake by Kuppfer cells in the liver. Minimal amounts of D-Cy5 were detected in the heart, due to its high vascularization and contact with blood. Other studies have shown higher uptake in lung and heart at shorter times, but dendrimer appears to get cleared away within 24 h. Interestingly, the brain does not show appreciable accumulation of dendrimer, which corresponds with our previous findings including the use of PET imaging where we have reported that these dendrimers do not cross an intact BBB in healthy kits.[13]

Effect of Neuroinflammation on Biodistribution

In neonatal rabbits with CP, we have previously shown that: (a) there is appreciable BBB impairment in the periventricular region as manifested by Evans blue extravasation and reduced expression of Occludin, a tight junction protein,[13] (b) the microglia and astrocytes become activated, making them more phagocytic, (c) this dendrimer shows brain uptake, followed by further selective accumulation in activated microglia and astrocytes based on immunohistochemical studies.[13] Newborn rabbits were used for this study due to our previous studies in neonatal rabbit model of CP where we have demonstrated efficacy using

dendrimer–drug conjugates. We explored how this difference in pathology correlates with difference in quantitative brain uptake of this dendrimer. Comparison of the brain uptake of D-Cy5 in healthy and CP newborn rabbits (day 1) indicates a 20-fold higher brain uptake of the D-Cy5 in CP kits, while there was no appreciable difference of its clearance and accumulation in other major organs (Table 2 and Figure 8). The basal levels of D-Cy5 observed in the brain of healthy rabbits with the help of FLS may have resulted from the presence of D-Cy5 in the choroid plexus, but not in the brain parenchyma. These basal levels (~0.003% of the injected dose) are above the detection limit of this method and suggest that this quantification assay can be sensitive enough to detect accumulation even less than 0.01% of ID. Since the dendrimers are mostly cleared from circulation in 24 h, vascular correction to the brain uptake levels does not change the uptake values.[38,39] Themean uptake of 0.06%in the brain of CP animals is qualitatively consistent with that of nontargeted nanoparticles that showed significant brain uptake in the presence of BBB impairment. However, most nanoparticles do not diffuse well in the parenchyma to be effective, unless densely PEG-coated.[40] However, PEG coating may prevent BBB transport and cellular localization. Interestingly, we have previously shown that these dendrimers not only cross the BBB but also selectively localize in the activated microglia and astrocytes, which are directly implicated in this neuroinflammation-induced CP model. This cellular accumulation, especially in the injured periventricular region, may explain the significant and dramatic efficacies and motor function improvement obtained with the dendrimer-*N*-acetyl cysteine conjugates in this CP model.[13]

This is the first study of dendrimer biodistribution and brain uptake quantification in a clinically relevant, *neonatal* brain injury model. With the exception of the report demonstrating that gadolinium-labeled, generation 6 PAMAM dendrimers injected interstitially are readily taken up by the deep lymphatic system in both mouse and pig models, providing MRI contrast,[41] previous studies of dendrimer biodistribution have typically involved adult rodents. Previous studies of PAMAM dendrimers in large animals indicated an opportunity for preoperative lymphatic mapping for surgical planning and the study of lymphangiogenesis in humans.[41] In this study, a rabbit model of neonatal/pediatric brain injury is used to evaluate dendrimer biodistribution. Based on these results, the distribution and clearance of D-Cy5 appeared to be similar to that seen in previously published adult models, indicating that this may be a viable platform for delivery of therapeutics for pediatric disorders.

CONCLUSIONS

We have developed a sensitive method for determination of the concentration of PAMAM dendrimers in tissue samples as well as blood serum and urine. The quantification was achieved using fluorescent labeling with a photostable Cy5 dye, which provided excellent sensitivity, reaching the limit of detection of 100 pg of D-Cy5 per 1 g of tissue based on FLS. The use of the near-IR dye enabled us to minimize potential influence of background tissue autofluorescence. The biodistribution results in major organs and serum compare well with prior results using radiolabeling. Using fluorescence labeling, both cellular biodistribution and pharmacokinetic studies can be performed, and samples can be stored as long as necessary without any precautions as in the case of radioactive materials. The present method may enable quantitative biodistribution and tissue imaging with the same agent, without the need for additional labeling. We quantified the differences in biodistribution of the dendrimer, in the presence of neuroinflammation, in our rabbit model of CP. There was a 20-fold increase in the dendrimer uptake in the periventricular region, which is the injured area of the brain in this model. Even though the brain uptake is small compared to the injected dose, the regional and cellular specificity achieved with these nonligand targeted dendrimers, may explain the dramatic efficacy observed upon

dendrimer–drug treatment in CP.[13] The biodistribution in the other organs, in animals with CP, were not significantly different compared to healthy animals.

Supplementary Material

Refer to Web version on PubMed Central for supplementary material.

Acknowledgments

This research was supported in part by the Perinatology Research Branch, Division of Intramural Research, Eunice Kennedy Shriver National Institute of Child Health and Human Development (NICHD), NIH, and by NICHD R01HD069562-02 (S.K.).

ABBREVIATIONS

Cy5	near-IR cyanine dye
D-Cy5	Cy5-labeled generation-4 hydroxyl-terminated PAMAM dendrimer
CP	cerebral palsy
FLS	florescence spectroscopy
HPLC	high-performance liquid chromatography
SEC	size exclusion chromatography
LOD	limit of detection

References

1. Lee CC, Gillies ER, Fox ME, Guillaudeu SJ, Fréchet JM, Dy EE, Szoka FC. A single dose of doxorubicin-functionalized bowtie dendrimer cures mice bearing C-26 colon carcinomas. Proc Natl Acad Sci USA. 2006; 103(45):16649–16654. [PubMed: 17075050]
2. Kukowska-Latallo JF, Candido KA, Cao Z, Nigavekar SS, Majoros IJ, Thomas TP, Balogh LP, Khan MK, Baker JR Jr. Nanoparticle targeting of anticancer drug improves therapeutic response in animal model of human epithelial cancer. Cancer Res. 2005; 65:5317–5324. [PubMed: 15958579]
3. Khan MK, Minc DL, Nigavekar SS, Kariapper MTS, Nair BM, Schipper M, Cook CA, Lesniak WG, Balogh LP. Fabrication of radioactive gold/dendrimer composite nanodevices and their use for nano-brachytherapy. Nanomed Nanotechnol. 2008; 4(1):57–69.
4. Lesniak WG, Kariapper MST, Nair BM, Balogh LP, Khan MK. Synthesis and characterization of PAMAM dendrimer-based multifunctional nanodevices for targeting $\alpha_v\beta_3$ integrins. Bioconjugate Chem. 2007; 18(4):1148–1154.
5. Venditto VJ, Regino CA, Brechbiel MW. PAMAM dendrimer based macromolecules as improved contrast agents. Mol Pharmaceutics. 2005; 2(4):302–311.
6. Wang X, Cai X, Hu J, Shao N, Wang F, Zhang Q, Xiao J, Cheng Y. Glutathione-triggered “off–on” release of anticancer drugs from dendrimer-encapsulated gold nanoparticles. J Am Chem Soc. 2013; 135:9805–9810. [PubMed: 23789713]
7. Shukla R, Thomas TP, Peters JL, Desai AM, Kukowska-Latallo J, Patri AK, Kotlyar A, Baker JR Jr. HER2 specific tumor targeting with dendrimer conjugated anti-HER2 mAb. Bioconjugate Chem. 2006; 17(5):1109–1115.
8. Majoros IJ, Myc A, Thomas T, Mehta CB, Baker JR Jr. PAMAM dendrimer-based multifunctional conjugate for cancer therapy: synthesis characterization and functionality. Biomacromolecules. 2006; 7(2):572–579. [PubMed: 16471932]
9. Patil ML, Zhang M, Taratula O, Garbuzenko OB, He H, Minko T. Internally cationic polyamidoamine PAMAM-OH dendrimers for siRNA delivery: effect of the degree of quaternization and cancer targeting. Biomacromolecules. 2009; 10(2):258–66. [PubMed: 19159248]

10. Talanov VS, Regino CA, Kobayashi H, Bernardo M, Choyke PL, Brechbiel MW. Dendrimer-based nanoprobe for dual modality magnetic resonance and fluorescence imaging. Nano Lett. 2006; 6(7):1459–1463. [PubMed: 16834429]
11. Thommey TP, Sascha N, Majoros IJ, Kotlyar A, Cao Z, Leroueil PR, Baker JR Jr. Folate-targeted nanoparticles show efficacy in the treatment of inflammatory arthritis. Arth Rheum. 2011; 63(9): 2671–2680. [PubMed: 21618461]
12. Chandrasekar D, Sistla R, Ahmad FJ, Khar RK, Diwan PV. The development of folate-PAMAM dendrimer conjugates for targeted delivery of anti-arthritic drugs and their pharmacokinetics and biodistribution in arthritic rats. Biomaterials. 2007; 3(28):504–512. [PubMed: 16996126]
13. Kannan S, Dai H, Navath RS, Balakrishnan B, Jyoti A, Janisse J, Romero R, Kannan RM. Dendrimer-based postnatal therapy for neuroinflammation and cerebral palsy in a rabbit model. Sci Trans Med. 2012; 4(130):130–146.
14. Iezzi R, Guru BR, Glybina IV, Mishra MK, Kennedy A, Kannan RM. Dendrimer-based targeted intravitreal therapy for sustained attenuation of neuroinflammation in retinal degeneration. Biomaterials. 2012; 33(3):979–988. [PubMed: 22048009]
15. Dai H, Navath RS, Balakrishnan B, Guru BR, Mishra MK, Romero R, Kannan RM, Kannan S. Intrinsic targeting of inflammatory cells in the brain by polyamidoamine dendrimers upon subarachnoid administration. Nanomedicine. 2010; 5(9):1317–1329. [PubMed: 21128716]
16. Shaunak S, Thomas S, Gianasi E, Godwin A, Jones E, Teo I, Mireskandari K, Luthert P, Duncan R, Patterson S, Khaw P, Brocchini S. Polyvalent dendrimer glucosamine conjugates prevent scar tissue formation. Nat Biotechnol. 2004; 22:977–984. [PubMed: 15258595]
17. Kim ID, Shin JH, Kim SW, Choi S, Ahn J, Han PL, Park JS, Lee JK. Intranasal delivery of HMGB1 siRNA confers target gene knockdown and robust neuroprotection in the postischemic brain. Mol Ther. 2012; 20(4):829–39. [PubMed: 22252450]
18. Mishra M, Kotta K, Hali M, Wykes S, Benchaala I, Gerard H, Hudson A, Whittum-Hudson J, Kannan RM. PAMAM dendrimer-azithromycin conjugate nanodevices for the treatment of Chlamydia trachomatis Infections. Nanomedicine. 2011; 7(6):935–944. [PubMed: 21658474]
19. Bosnjakovic A, Mishra M, Ren W, Kurtoglu YE, Kannan RM. Poly(amidoamine) dendrimer-erythromycin conjugates for drug delivery to macrophages involved in periprosthetic inflammation. Nanomedicine. 2010; 7(3):284–294. [PubMed: 21059404]
20. Chauhan AS, Diwan PV, Jain NK, Tomalia DA. Unexpected in vivo anti-inflammatory activity observed for simple, surface functionalized poly(amidoamine) dendrimers. Biomacromolecules. 2009; 11(5):1195–202. [PubMed: 19348417]
21. Medina SH, Tiruchinapally G, Chevliakov MV, Durmaz YY, Stender RN, Ensminger WD, Shewach DS, Elsayed ME. Targeting hepatic cancer cells with PEGylated dendrimers displaying N-acetylgalactosamine and SP94 peptide ligands. Adv Healthcare Mater. 2013; 2:1337–1350.
22. Kasturirangan V, Nair BM, Kariapper MT, Lesniak WG, Tan W, Bizimungu R, Kanter P, Toth K, Buitrago S, Rustum YM, Hutson A, Balogh LP, Khan MK. *In vivo* toxicity evaluation of gold-dendrimer composite nanodevices with different surface charges. Nanotoxicology. 2013; 7(4): 441–51. [PubMed: 22394369]
23. Nair BM, Kariapper MTS, Lesniak WG, Tan W, Hutson A, Khan MK, Balogh LP. Toxicity evaluation of gold-dendrimer composite nanodevices *in vitro* - difference found between tumor and proliferating endothelial cells. Nanotoxicology. 2009; 3(2):139–151.
24. Mager ED, Mody V, Xu C, Forrest A, Lesniak WG, Nigavekar SS, Kariapper TM, Minc L, Khan MK, Balogh LP. Physiologically based pharmacokinetic model for composite nanodevices: effect of charge and size on in vivo disposition. Pharm Res. 2012; 29(9):2534–2542. [PubMed: 22688900]
25. Khan MK, Nigavekar SS, Kariapper MST, Nair BM, Lesniak WG, Balogh LP. Host-guest nanodevices: *in vivo* biodistribution of dendrimers and dendrimer nanocomposites - implications for cancer imaging and therapy. Technol Cancer Res Treat. 2005; 4(6):603–613. [PubMed: 16292880]
26. Balogh L, Nigavekar SS, Nair BM, Lesniak W, Zhang C, Sung LY, Kariapper MS, El-Jawahri A, Llanes M, Bolton B, Mamou F, Tan W, Hutson A, Minc L, Khan MK. Significant effect of size on

the in vivo biodistribution of gold composite nanodevices in mouse tumor models. Nanomedicine. 2007; 3(4):281–296. [PubMed: 17962085]

27. Sadekar S, Ray A, Janàt-Amsbury M, Peterson CM, Ghandehari H. Comparative biodistribution of PAMAM dendrimers and HPMA copolymers in ovarian-tumor-bearing mice. Biomacromolecules. 2011; 12(1):88–96. [PubMed: 21128624]
28. Malik N, Wiwattanapatapee R, Klopsch R, Lorenz K, Frey H, Weener JW, Meijer EW, Paulus W, Duncan R. Dendrimers: Relationship between structure and biocompatibility in vitro, and preliminary studies on the biodistribution of ^{125}I-labelled polyamidoamine dendrimers in vivo. J Controlled Release. 2000; 65(1–20):133–148.
29. Kojima C, Regino C, Umeda Y, Kobayashi H, Kono K. Influence of dendrimer generation and polyethylene glycol length on the biodistribution of PEGylated dendrimers. Int J Pharmaceutics. 2010; 383(1–2):293–296.
30. Nigavekar SS, Sung LY, Llanes M, El-Jawahri A, Lawrence TS, Becker CW, Balogh L, Khan MK. 3H dendrimer nanoparticle organ/tumor distribution. Pharm Res. 2004; 21(3):476–483. [PubMed: 15070099]
31. Li Y, He H, Jia X, Lu WL, Lou J, Wei Y. A dual-targeting nanocarrier based on poly(amidoamine) dendrimers conjugated with transferrin and tamoxifen for treating brain gliomas. Biomaterials. 2012; 33(15):3899–908. [PubMed: 22364698]
32. Kannan S, Saadani-Makki F, Balakrishnan B, Chakraborty P, Janisse J, Lu X, Muzik O, Romero R, Chugani DC. Magnitude of [(11)C]PK11195 binding is related to severity of motor deficits in a rabbit model of cerebral palsy induced by intrauterine endotoxin exposure. Dev Neurosci. 2011; 33(3–4):231–40. [PubMed: 21791891]
33. Klajnert B, Sadowska M, Bryszewska M. Fluorescence studies on PAMAM dendrimers interactions with bovine serum albumin. Bioelectrochemistry. 2004; 55(1–2):23–26. [PubMed: 15522688]
34. Shcharbin D, Klajnert B, Mazhul V, Bryszewska MJ. Dendrimer interactions with hydrophobic fluorescent probes and human serum albumin. J Fluoresc. 2005; 15(1):21–28. [PubMed: 15711873]
35. Klajnert B, Bryszewska M. Fluorescence studies on PAMAM dendrimers interactions with bovine serum albumin. Bioelectrochemistry. 2002; 55:33–35. [PubMed: 11786335]
36. Kobayashi H, Kawamoto S, Jo SK, Sato N, Saga T, Hiraga A, Konishi J, Hu S, Togashi K, Brechbiel MW. Renal tubular damage detected by dynamic micro-MRI with a dendrimer-based magnetic resonance contrast agent. Kidney Int. 2002; 61(6):1980–1985. [PubMed: 12028438]
37. Dear JW, Kobayashi H, Brechbiel MW, Star RA. Imaging acute renal failure with polyamine dendrimer-based MRI contrast agents. Nephron Clin Pract. 2006; 103(2):c45–c49. [PubMed: 16543755]
38. van Rooy I, Cakir-Tascioglu S, Hennink WE, Storm G, Schiffelers RM, Mastrobattista E. In vivo methods to study uptake of nanoparticles into the brain. Pharm Res. 2011; 28(3):456–71. [PubMed: 20924653]
39. Calvo P, Gouritin B, Villarroya H, Eclancher F, Giannavola C, Klein C, Andreux JP, Couvreur P. Quantification and localization of PEGylated polycyanoacrylate nanoparticles in brain and spinal cord during experimental allergic encephalomyelitis in the rat. Eur J Neurosci. 2002; 15(8):1317–26. [PubMed: 11994126]
40. Nance EA, Woodworth GF, Sailor KA, Shih TY, Xu Q, Swaminathan G, Xiang D, Eberhart C, Hanes J. A dense poly(ethylene glycol) coating improves penetration of large polymeric nanoparticles within brain tissue. Sci Transl Med. 2012; 4(149):149–119.
41. Sena LM, Fishman SJ, Jenkins KJ, Xu H, Brechbiel MW, Regino CA, Kosaka N, Bernardo M, Choyke PL, Kobayashi H. Magnetic resonance lymphangiography with a nano-sized gadolinium-labeled dendrimer in small and large animal models. Nanomedicine. 2010; 5(8):1183–1191. [PubMed: 21039196]

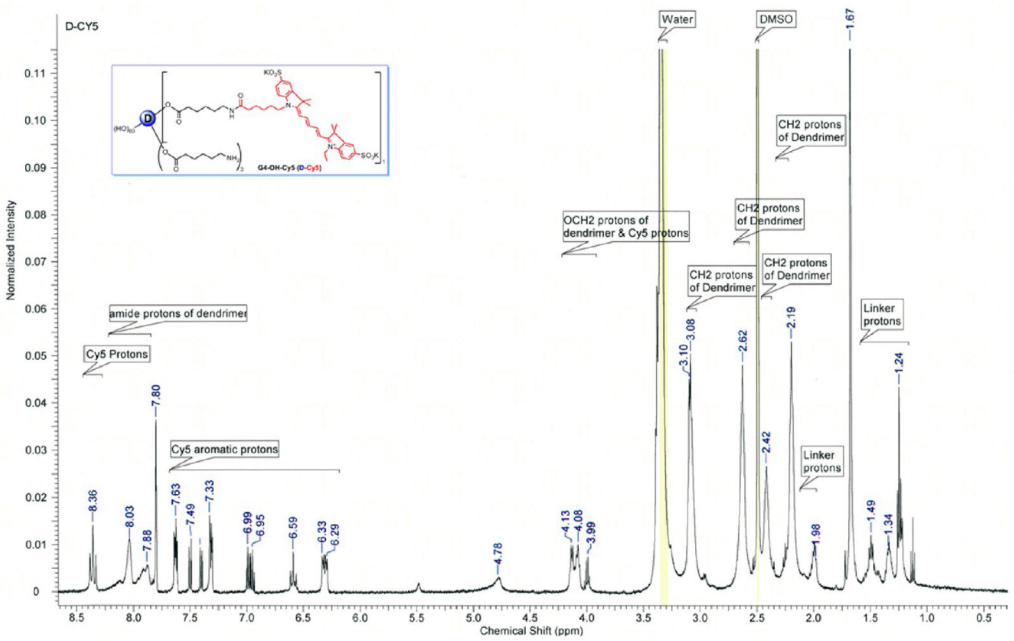

Figure 1.

^{1}H NMR of the dendrimer-Cy5 (D-Cy5) conjugate in DMSO-d_6, showing the presence of all components of the D-Cy5 conjugate (dendrimer, linker, and dye).

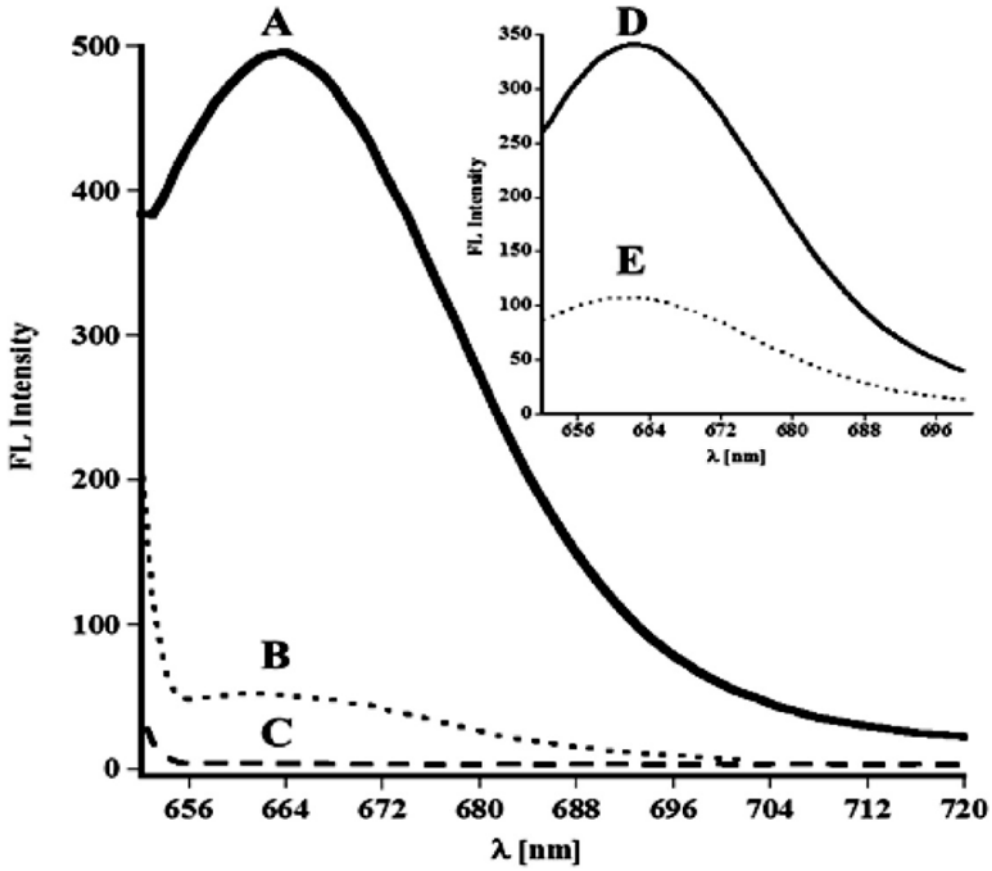

Figure 2.

Example of the florescence spectra used for determination of D-Cy5 and Cy5 in kidneys 24 h post injection: A (solid line), rabbit injected D-Cy5; B (dotted line), rabbit injected with Cy5; C (dashed line), control nontreated rabbit. Inset D (solid line), D-Cy5 at concentration of 2 μg/mL and E (dotted line), Cy5 at concentration of 0.25 μg/mL. The apparent increase of fluorescence intensity is related to the presence of fluorophore, and results indicate much higher accumulation of D-Cy5 than free Cy5.

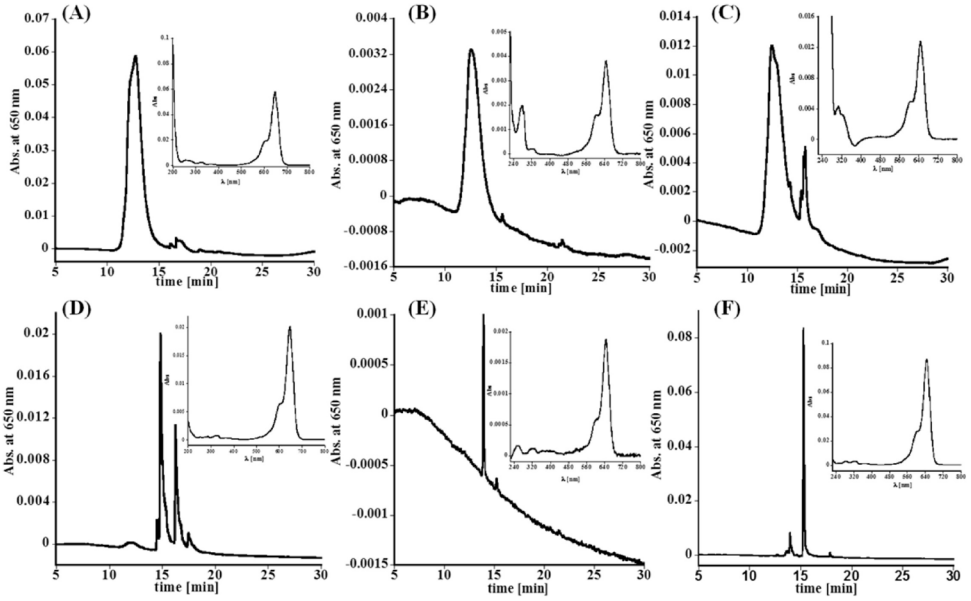

Figure 3.

Representative HPLC chromatograms acquired based on absorbance at 650 nm for: (A) D-Cy5 conjugate, (B) kidney extract, and (C) urine obtained from rabbit 24 h post injection of D-Cy5, (D) Cy5, (E) kidney extract, and (F) urine acquired from rabbit 24 h post injection of the dye. Insets, UV–vis spectra recoded under peaks related to D-Cy5 and Cy5 in samples used as standards, kidney extracts, and urine. Results indicated the presence of D-Cy5, and relatively low levels of free, released dye, in specimens collected from rabbit treated with the conjugate. Relatively low Cy5 levels were detected in animals injected with free Cy5.

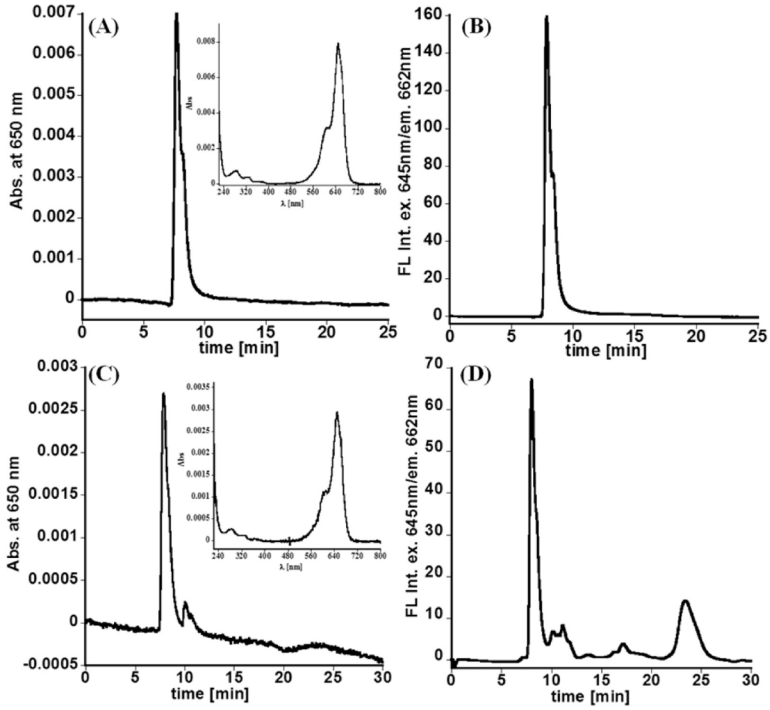

Figure 4.

Size exclusion chromatograms of D-Cy5 conjugate obtained based on (A) absorbance at 650 nm (insert UV–vis spectrum obtained under the peak) and (B) fluorescence with excitation of 645 nm and emission at 665 nm. The same retention time was observed for unlabeled dendrimer. Results clearly demonstrate covalent attachment of Cy5 to the dendrimer. (C) Absorbance at 650 nm and (D) fluorescence SEC chromatograms obtained using extract from kidney acquired from rabbit 24 h post administration of the D-Cy5 conjugate. Similarly to HPLC, SEC confirmed the presence of D-Cy5 in the kidney.

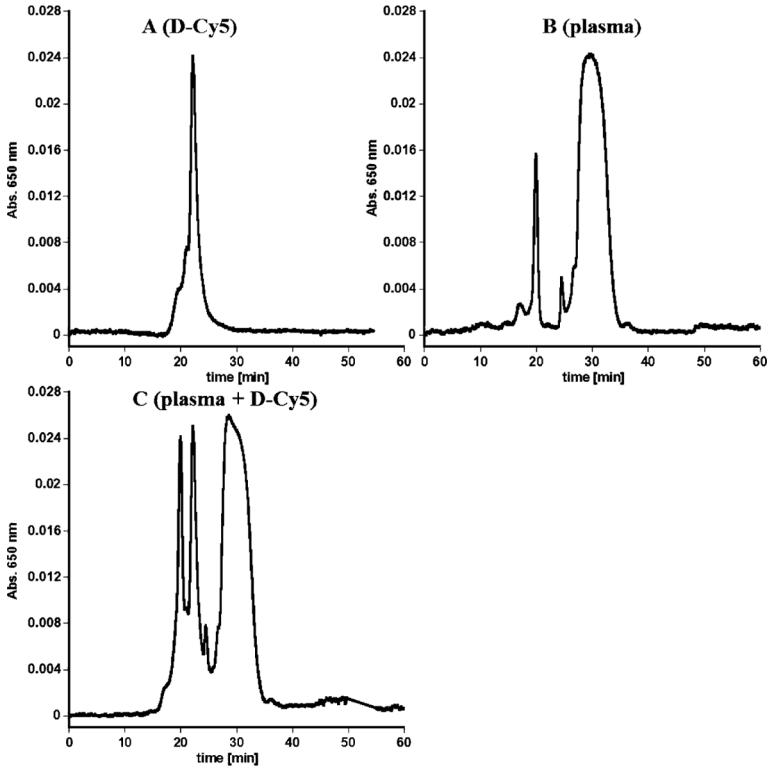

Figure 5.

Size exclusion chromatograms of: (A) D-Cy5, (B) plasma, and (C) physical mixture of D-Cy5 and plasma, obtained 10 min after mixing. The same chromatogram was obtained 24 h incubation at 37 °C, indicating that D-Cy5 was stable in plasma and did not formed aggregates with plasma constituents under experimental condition and detectable by this method.

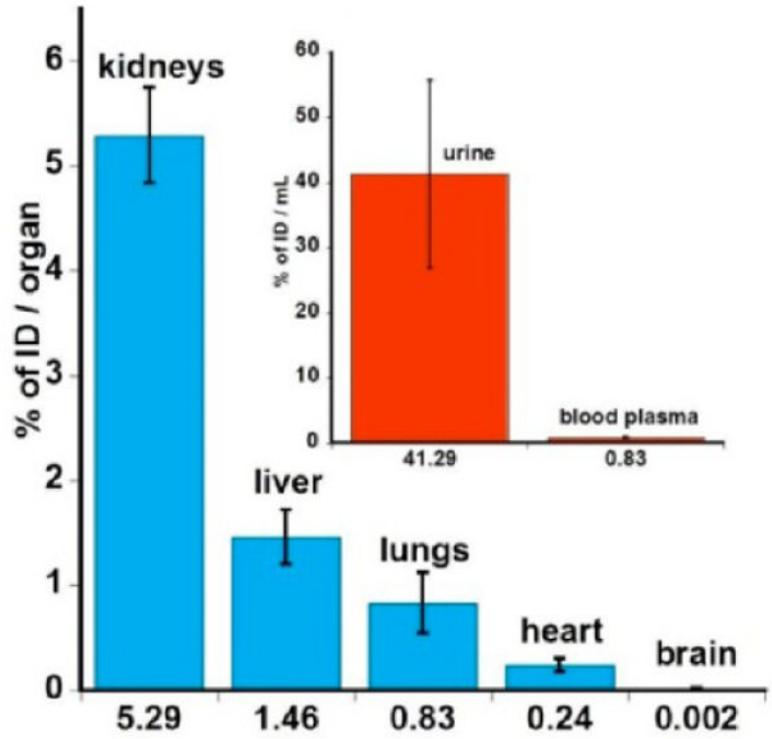

Figure 6.
Biodistribution of D-Cy5 in major organs of neonatal rabbits as well as blood plasma and urine (insert) 24 h post injection, expressed as percentage of injected dose of D-Cy5 per organs and per mL, respectively. Results acquired for the D-Cy5 conjugate indicate fast renal clearance, high concentration in urine obtained from bladder, and minor involvement of RES.

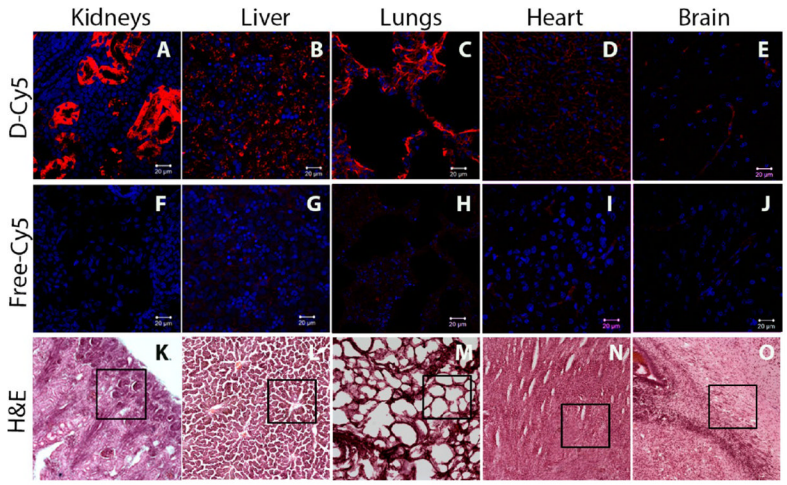

Figure 7.

Biodistribution of D-Cy5 and free Cy5 in the major organs 24 h post i.v. injection in the neonatal rabbit. Confocal micrographs showing the accumulation of D-Cy5 and free Cy5 in kidney (A, F), liver (B, G), lung (C, H), heart (D, I), and brain (E, J) of neonatal rabbits assessed 24 h post i.v. injection. Images clearly indicate that the kidneys, liver, and lungs have a much higher accumulation of dendrimer compared to free dye. On the contrary, the brain does not exhibit any accumulation of dendrimer, which is in good agreement with HPLC, SEC, and FLS based quantification results (Figure 6). Scale bars: 20 μm. Low magnification (10×) H&E images showing the representative area used for imaging dendrimers under confocal microscope. Scale bar: 100 μm.

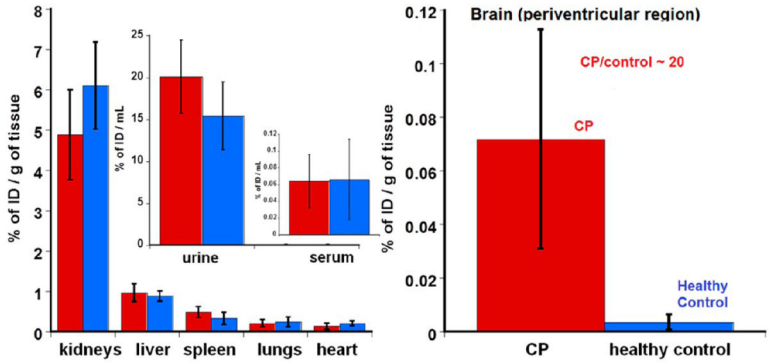

Figure 8.

Biodistribution of D-Cy5 conjugate in control (blue bars) and CP (red bars) newborn rabbits (day 1 of life) 24 h post injection. Results indicate significantly higher brain uptake of D-Cy5 in CP kits compared to control. However, there is no difference in its accumulation in major peripheral organs and excretion between both groups.

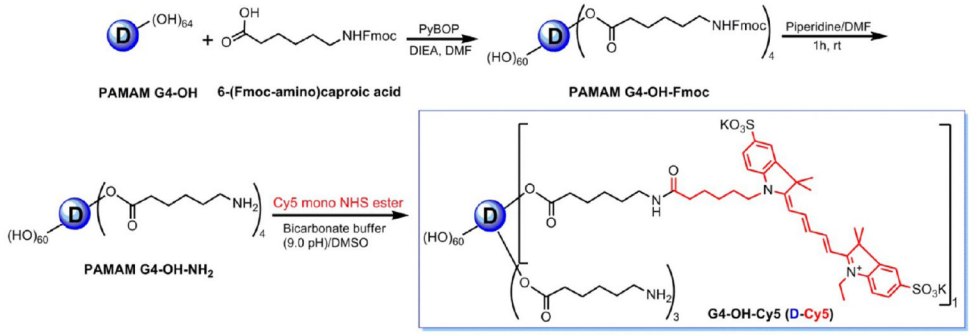

Scheme 1.
Schematic Representation of the Synthesis of D-Cy5 Conjugate

Table 1

Comparison of the Biodistribution of D-Cy5 and Cy5 in Neonatal Rabbits (day 5 of life), 24 h Post Administration[a]

	D-Cy5 content in tissue (μg/g)			Cy5 content (μg/g) of tissue ± std.	
	determined by FLS	**determined by HPLC**	**determined by SEC**	**determined by FLS**	**determined by HPLC**
kidneys	37.1 ± 3.01	31. ± 4.81	34.1 ± 7.12	0.13 ± 0.06	0.2 ± 0.09
heart	4.78 ± 0.38	3.85 ± 0.32	2.81 ± 0.22	0.37 ± 0.08	0.28 ± 0.06
lungs	5.23 ± 0.62	6.22 ± 1.01	2.95 ± 0.73	0.14 ± 0.012	0.18 ± 0.09
liver	5.72 ± 1.59	5.1 ± 1.79	3.99 ± 1.7	0.19 ± 0.05	0.25 ± 0.1
brain	0.003 ± 0.001	under LOD	under LOD	0.008 ± 0.0009	under LOD
serum	7.45 ± 1.8	5.8 ± 2.08	6.2 ± 1.8	0.47 ± 0.071	0.39 ± 0.08
urine	277 ± 46	251 ± 17	263 ± 89	13.3 ± 1.95	7.94 ± 2.52

[a]One group of rabbits (n = 5) was injected with 0.8 mg of the conjugate and other with 0.03 mg of free dye.

FLS = fluorescence spectroscopy, HPLC = high-performance liquid chromatography, SEC = size exclusion chromatography, LOD = limit of detection. Traces of free Cy5 were detected only in kidney and urine obtained from rabbits injected with D-Cy5, which indicates that conjugate was stable *in vivo*. Urine samples were obtained directly from the bladder by pressing abdominal and pelvic cavity before animals were sacrificed.

Table 2

Biodistribution of D-Cy5 in Neonatal Rabbits (day 1 of life), 24 h Post Administration of 0.8 mg of D-Cy5 (n = 5 for Control and n = 3 for CP Animals)[a]

specimen	healthy control	CP
kidneys	49 ± 9	39 ± 9
liver	7.02 ± 0.41	7.64 ± 0.56
spleen	2.66 ± 0.53	3.79 ± 0.21
lungs	2.07 ± 0.36	1.67 ± 0.22
heart	1.68 ± 0.37	1.06 ± 0.48
brain	0.03 ± 0.02	0.57 ± 0.33
blood	0.54 ± 0.1	0.51 ± 0.17
urine	160 ± 35	165 ± 32

[a]Tissue concentrations of D-Cy5 are in μg/g of tissue and for blood and urine in μg/mL.